

Article

Theoretical Approach for the Luminescent Properties of Ir(III) Complexes to Produce Red–Green–Blue LEC Devices

Mireya Santander-Nelli ^{1,2,*} , Bastián Boza ³, Felipe Salas ³, David Zambrano ⁴ , Luis Rosales ⁴ and Paulina Dreyse ^{3,*}

¹ Advanced Integrated Technologies (AINTECH), Chorrillo Uno, Parcela 21, Lampa, Santiago 9390015, Chile

² Centro Integrativo de Biología y Química Aplicada (CIBQA), Universidad Bernardo O'Higgins, General Gana 1702, Santiago 8370854, Chile

³ Departamento de Química, Universidad Técnica Federico Santa María, Avda. España 1680, Casilla, Valparaíso 2390123, Chile; bastian.boza.14@sansano.usm.cl (B.B.); felipe.salasc@usm.cl (F.S.)

⁴ Departamento de Física, Universidad Técnica Federico Santa María, Avda. España 1680, Casilla, Valparaíso 2390123, Chile; david.zambrano@usm.cl (D.Z.); luis.rosalesa@usm.cl (L.R.)

* Correspondence: ms@aintech.cl (M.S.-N.); paulina.dreyse@usm.cl (P.D.)

Abstract: With an appropriate mixture of cyclometalating and ancillary ligands, based on simple structures (commercial or easily synthesized), it has been possible to design a family of eight new Ir(III) complexes (**1A**, **1B**, **2B**, **2C**, **3B**, **3C**, **3D** and **3E**) useful as luminescent materials in LEC devices. These complexes involved the use of phenylpyridines or fluorophenylpyridines as cyclometalating ligands and bipyridine or phenanthroline-type structures as ancillary ligands. The emitting properties have been evaluated from a theoretical approach through Density Functional Theory and Time-Dependent Density Functional Theory calculations, determining geometric parameters, frontier orbital energies, absorption and emission energies, injection and transport parameters of holes and electrons, and parameters associated with the radiative and non-radiative decays. With these complexes it was possible to obtain a wide range of emission colours, from deep red to blue (701–440 nm). Considering all the calculated parameters between all the complexes, it was identified that **1B** was the best red, **2B** was the best green, and **3D** was the best blue emitter. Thus, with the mixture of these complexes, a dual host–guest system with **3D-1B** and an RGB (red–green–blue) system with **3D-2B-1B** are proposed, to produce white LECs.

Keywords: Ir-iTMC; LEC devices; TD-DFT; phosphorescence; RGB



Citation: Santander-Nelli, M.; Boza, B.; Salas, F.; Zambrano, D.; Rosales, L.; Dreyse, P. Theoretical Approach for the Luminescent Properties of Ir(III) Complexes to Produce Red–Green–Blue LEC Devices. *Molecules* **2022**, *27*, 2623. <https://doi.org/10.3390/molecules27092623>

Academic Editors: Sergey A. Adonin and Artem L. Gushchin

Received: 18 March 2022

Accepted: 12 April 2022

Published: 19 April 2022

Publisher's Note: MDPI stays neutral with regard to jurisdictional claims in published maps and institutional affiliations.



Copyright: © 2022 by the authors. Licensee MDPI, Basel, Switzerland. This article is an open access article distributed under the terms and conditions of the Creative Commons Attribution (CC BY) license (<https://creativecommons.org/licenses/by/4.0/>).

1. Introduction

The concept of Solid-State Lighting (SSL) promotes energy savings and greenhouse gas reduction compared to conventional lighting (incandescent bulbs or halogen lamps) [1,2]. The most common SSL devices are LED (Light Emitting Diode) and OLED (Organic Light Emitting Diode) [3,4]. LED technology is based on high purity inorganic semiconductors, for example: AlGaAs, InGaN, GaN, and ZnSe, among others. These materials provide highly efficient and convenient point sources of light of different colors, depending on the semiconductor used [3]. Instead, OLEDs are processed in a multilayer system, using neutral organic or organometallic luminescent compounds, sandwiched between two electrodes [5–7]. To improve the manufacturing, costs, and performance of these SSLs, LECs (Light Emitting Electrochemical Cells) emerge as a promising alternative [8].

All SSL systems work through electron–hole recombination processes, where electrons are injected from the cathode into the luminescent material and holes are injected from the anode into the luminescent material. The recombination zone must take place in the middle of the luminescent material, producing an exciton, which if radiatively deactivated could produce light [9–12]. LEC devices contain a thin film of an ionic luminescent material

between a cathode and an anode. This material is usually an ionic transition metal complex (iTMC) [13,14] and their films can be easily processed from an organic solution, using the spin-coating technique, which provides thinner and homogeneous layers [15]. Due to the ionic nature of the iTMC (unlike neutral compounds used in OLEDs), multilayer arrangements are not required in LEC because the electron–hole recombination is determined by the ionic mobility of the active molecules; therefore, LECs are a low cost alternative compare to OLEDs [16].

The cyclometalated Ir(III) complexes ($[\text{Ir}(\text{C}^{\wedge}\text{N})_2(\text{N}^{\wedge}\text{N})]^+$, where $\text{C}^{\wedge}\text{N}$ is a cyclometalating ligand and $\text{N}^{\wedge}\text{N}$ is an ancillary ligand) show the best performance as luminescent material in LECs [17–19]. The Ir atom is characterized by a high ligand-field splitting energy, thus in their complexes the metal centered (MC) excited states are less thermally accessible, avoiding the non-radiative decays [20,21]. Besides, the spin–orbit coupling (SOC) is increased in Ir-iTMC compared to complexes with metals of the 1st or 2nd transition rows, thus, a very effective singlet-to-triplet intersystem crossing occurs in Ir-iTMC, promoting radiative decay with a high quantum yield [22].

Another outstanding characteristic is that the Ir(III) complexes show emissions in a wide range of the visible spectrum, which can be modulated by the incorporation of an electron donor and/or acceptor substituents in both $\text{C}^{\wedge}\text{N}$ and $\text{N}^{\wedge}\text{N}$ ligands [22–24]. This can be understood since the electron density distributions of the frontier molecular orbitals (HOMO: Highest Occupied Molecular Orbital, and LUMO: Lowest Unoccupied Molecular Orbital) are similar in most of the Ir-iTMCs [23,25]. The HOMO has contributions from Ir $d\pi$ orbitals and π orbitals of the $\text{C}^{\wedge}\text{N}$ ligand, and the LUMO is composed mainly of π^* orbitals centered in the $\text{N}^{\wedge}\text{N}$ ligand [22,23,26]. Consequently, the emitting triplet state (T_1) commonly has a ${}^3\text{MLCT}/{}^3\text{LLCT}$ (MLCT: metal-to-ligand charge transfer, LLCT: ligand-to-ligand charge transfer, from $\text{C}^{\wedge}\text{N}$ to $\text{N}^{\wedge}\text{N}$) mixed character [22,23,25,26]. The modulation of the emission energy involves, for example, the use of electron-withdrawing substituents in the $\text{C}^{\wedge}\text{N}$ ligand, decreasing the electron density on the metal, leading to the stabilization of the HOMO level. Also, electron donor substituents can be incorporated into the $\text{N}^{\wedge}\text{N}$ ligand, mainly destabilizing the LUMO. The HOMO–LUMO gap is increased with both strategies, obtaining high emission energies. Conversely, with the HOMO destabilization and LUMO stabilization, emissions at lower energies can be obtained [20,25,27].

The design of efficient Ir(III) complexes for LECs involve, in many cases, complicated synthetic procedures of the ligands, obtained at very low yields, affecting the final cost of the devices [19,28,29]. In this sense, the challenge to produce new Ir-iTMCs should involve the use of ancillary and cyclometalating ligands with favorable synthetic routes, providing specific emission colors and, of course, stable compounds.

Achieving full color displays, technologies and versatile lighting applications (lighting in public spaces, highways, advertising, etc.) with SSL devices, is one of the main challenges in the communication, lighting, and computer industries [30,31]. For this target, white light devices with high efficiency and a long lifetime are essential. White light emission from an LEC can be produced with RGB (red–green–blue) emitters, in a triple mix of materials in a single layer, containing the primary colors, since the white output light is a mixture of these three components [32–34]. Alternatively, it is possible to use an orange (O) emitter and a blue emitter as complementary colors to produce white light [35]. Since a wide range of colors have been achieved in LECs with Ir-iTMCs, the white light with blends of these complexes has also been explored [36–40]. These systems are called host–guest, where a blue and/or green emitter host is doped with a small concentration of a red emitter guest, in order to promote an incomplete energy transfer from the blue–green complex to excitate a red complex, giving white light from the mixture of the blue–green and red emissions [36–40]. One of the most cited studies that has used this strategy involves the use of $[\text{Ir}(\text{dfppz})_2(\text{dedaf})]^+$ (dfppz: 1-(2,4-difluorophenyl)-1H-pyrazole, dedaf: 9-diethyl-4,5-diazafluorene) as a blue–green emitter (emission at 491 nm) and $[\text{Ir}(\text{ppy})_2(\text{biq})]^+$ (ppy: 2-phenylpyridine, biq: 2,2-biquinoline) as a red emitter (emission at 672 nm), obtaining a white LEC with an external quantum efficiency (EQE) of 4% [36]. Another example

involved the use of $[\text{Ir}(\text{dfppz})_2(\text{dtb-bpy})]^+$ (dtb-bpy: 4,4'-di-tert-butyl-2,2'-bipyridine) as a blue–green complex (emission at 492 nm) and the same red $[\text{Ir}(\text{ppy})_2(\text{biq})]^+$ complex; however, it showed a low efficiency compared to the other case (EQE: 3.2%) [18]. The latter was improved using a mixture of $[\text{Ir}(\text{dfppz})_2(\text{dtb-bpy})]^+$ and $[\text{Ir}(\text{ppy})_2(\text{biq})]^+$, more an orange complex $[\text{Ir}(\text{ppy})_2(\text{dasb})]^+$ (dasb: 4,5-diaza-9,90-spirofluorene), increasing the EQE up to 6.3% [38].

Considering the wide range of emitting colors obtained from the Ir-ITMCs, the contributions to white light can be feasibly increased, exploring strategic blends of C[^]N and N[^]N ligands to produce new stable RGB Ir(III) complexes. According to the antecedents commented on, in this work are evaluated by theoretical calculations, the photophysical properties of an extended family of Ir(III) complexes (see Figure 1) with a mix of C[^]N and N[^]N ligands, with different electron-donating and/or -withdrawing natures and different structures to enhance the LEC performance. Therefore, the design of three series was carried out with the purpose of tuning the emitting color of the complexes, from red to blue, mainly determined by the cyclometalating ligand. In this sense, series 1 was expected to show a red emission; series 2, a green emission; and finally, series 3, a blue emission. However, some discrepancies were observed, namely, the 3E complex exhibits strongly green-shifted emissions, which will be discussed in more depth in this study.

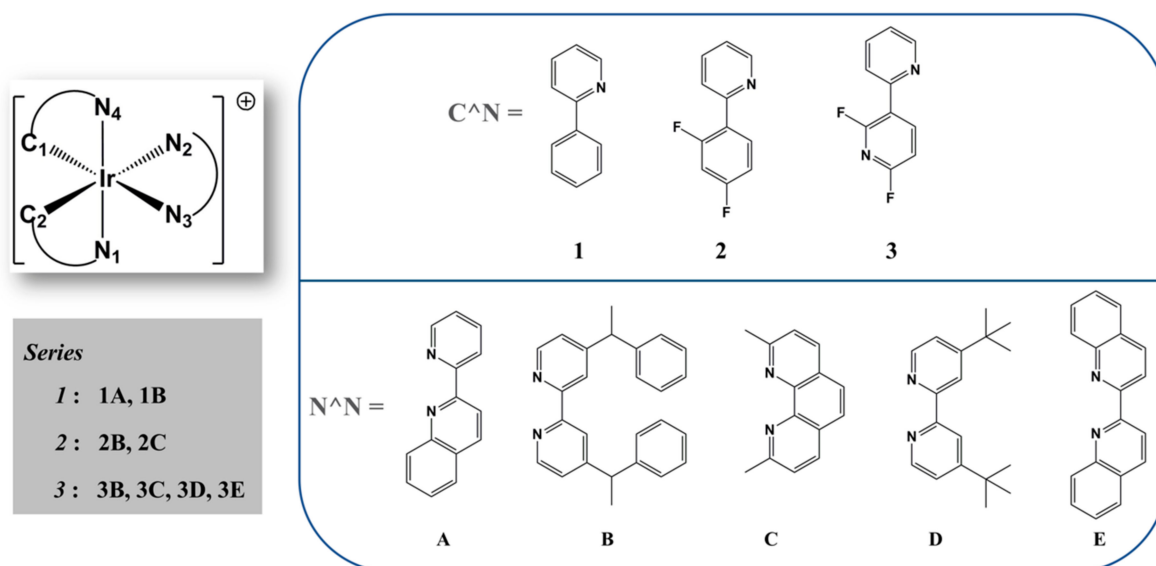


Figure 1. Molecular structures of the Ir(III) complexes studied. Labeling of the atoms coordinated with the metallic center is included to guide the description of the geometric parameters.

The calculations were carried out using the Density Functional Theory (DFT) level, providing a deep structural characterization of the ground and excited states, as well as a study of the absorption and emission properties, and the associated photophysical efficiency parameters, to identify the complexes with the best emitting properties. Finally, the best combinations of blue, green, and red emitters are proposed with the aim to contribute to the strategic design of white LECs.

2. Computational Details

All calculations were performed using the DFT approach with the B3LYP functional [41,42], which proved to be the most suitable to reproduce the absorption and emission properties of the $[\text{Ir}(\text{ppy})_2(\text{bpy})]^+$ complex, which was used as the reference complex for the DFT benchmark (see Table S1 of Supporting Information (SI)). The LANL2DZ [43] basis set and quasi-relativistic pseudopotential were adopted for the Iridium atom, while the 6-31G(d,p) [44,45] basis set was used for the other atoms. The optimized structures for all complexes correspond to the energy minima, according to the vibrational frequencies (real

values). The Time-Dependent DFT (TD-DFT) methodology was used to calculate the first 50 and 6 triplet excited states, respectively. The triplet (T_1) excited states were optimized using TD-DFT gradients (TD-DFT optimization). Emission energies were estimated as the vertical energy difference between the total energies of the relaxed triplet state and ground state at the optimized triplet geometry. The continuous solvent effect was incorporated by the IEF-PCM model (polarized continuum model), [46] using dichloromethane as the solvent. The optimized structures of 3MC states were also determined; for this purpose unrestricted triplet optimization calculations were performed on the bases of the geometry of the distorted excited triplet state, where the six coordinate bond lengths around the metal atom (Ir- C_{CN} , Ir- N_{CN} and Ir- N_{NN}) are all gradually elongated (up to about 0.8 Å) and spin density distribution calculations confirm that the metal-centered excited states are obtained, as described in the literature [47,48]. The ionization potentials (IP), the electron affinities (EA), and the hole/electron reorganization energies were obtained by the differences between the total energies of the molecular system in its fundamental state and with one more electron or one less electron [49–51]. All the calculations were performed in the Gaussian16 program package [52] and the wavefunction analyses were performed in the Multiwfn 3.4 code [53].

3. Results and Discussion

3.1. Molecular Geometries in the Ground States and Lowest Excited Triplet States

The different Ir(III) complexes studied are shown in Figure 1, with the numbering of some key atoms. According to this nomenclature, the selected geometric parameters of the ground states (S_0) and the excited triplet states (T_1 , T_2 or T_3) are summarized in Table 1. All the data of the determined geometric parameters are shown in Table S2 of the Supplementary Materials.

Table 1. Selected optimized geometric parameters of all complexes under study in the S_0 and triplet excited states (T_1 , T_2 or T_3) determined at the B3LYP/6-31G(d)-LANL2DZ level of theory.

	1A		1B		2B		2C	
	S_0	T_1	S_0	T_1	S_0	T_2	S_0	T_2
Bond length (Å)								
Ir-C ₁	2.02	2.02	2.02	1.99	2.02	2.01	2.02	2.02
Ir-C ₂	2.03	1.98	2.02	2.01	2.02	2.02	2.02	2.01
Ir-N ₁	2.08	2.08	2.07	2.07	2.07	2.04	2.09	2.10
Ir-N ₂	2.20	2.23	2.31	2.24	2.29	2.31	2.28	2.29
Ir-N ₃	2.32	2.24	2.31	2.27	2.30	2.30	2.29	2.31
Ir-N ₄	2.08	2.09	2.08	2.09	2.08	2.09	2.07	2.04
Bond angle (deg)								
C ₁ -Ir-N ₄	96.2	97.9	95.7	96.9	95.5	94.9	95.8	95.9
C ₁ -Ir-N ₃	169.4	164.4	177.1	175.9	177.5	177.2	172.2	172.6
C ₁ -Ir-C ₂	85.4	90.2	82.4	88.2	82.2	83.2	82.3	83.1
	3B		3C		3D		3E	
	S_0	T_2	S_0	T_3	S_0	T_2	S_0	T_2
Bond length (Å)								
Ir-C ₁	2.02	2.00	2.01	2.02	2.01	2.00	2.01	2.02
Ir-C ₂	2.01	2.02	2.02	2.02	2.01	2.00	2.02	2.02
Ir-N ₁	2.08	2.06	2.09	2.08	2.08	2.08	2.08	2.07
Ir-N ₂	2.29	2.20	2.28	2.23	2.19	2.18	2.29	2.22
Ir-N ₃	2.28	2.24	2.28	2.23	2.19	2.18	2.28	2.22
Ir-N ₄	2.08	2.10	2.09	2.09	2.08	2.08	2.09	2.10
Bond angle (deg)								
C ₁ -Ir-N ₄	95.7	96.5	95.6	95.5	95.5	96.9	95.5	94.9
C ₁ -Ir-N ₃	173.5	177.7	172.6	177.2	172.5	170.1	178.9	178.3
C ₁ -Ir-C ₂	81.7	85.0	81.7	82.6	89.0	94.5	82.1	83.9

The calculated data are in agreement with the bond lengths and angles reported in literature for similar cyclometalated Ir(III) complexes [15,19,54,55]. In the ground state it is possible to observe that all complexes have a distorted octahedral geometry around the Ir metallic center, and exhibit similar geometric parameters between them, namely, for the Ir-C and Ir-N bonds of the C[^]N ligand, an average length of 2.02 and 2.08 Å is found, respectively; while the Ir-N_N bond lengths are in the range of 2.19 and 2.32 Å. This is significantly longer than those for C[^]N, which is attributed to the strong *trans*-effect of the C donor in the C[^]N ligands, in agreement with the reported literature for the Ir(III) complexes with similar characteristics [56–59]. Furthermore, the bond angles involving the metallic center are also very similar between all complexes; the C₁-Ir-N₄ angle is ~96° and the C₁-Ir-N₃ angle is around 172–179° for all the complexes. Finally, the C₁-Ir-C₂ angle is in the range between 82–89°.

Comparing the geometric parameters of the triplet excited states with respect to the parameters of the S₀ structures, marginal variations are found in the distances between the metal center and the ligands; some significant variations were found for Ir-N_N (Ir-N₂ and Ir-N₃) in almost all complexes, where a shortening is identified in the excited states.

3.2. Frontier Molecular Orbitals Analysis

To understand the absorption and emission properties of the studied complexes, it is necessary to analyze their electronic structures in the ground state, namely: the electron distributions of HOMO and LUMO, the energies of the frontier orbitals, and HOMO–LUMO gaps (Δ HL). The contributions of molecular fragments to each molecular orbital (including energies) are summarized in Tables S3 and S4 of the Supplementary Materials. Figure 2 depicts the energy diagram showing the HOMO and LUMO surfaces and Δ HL of all complexes.

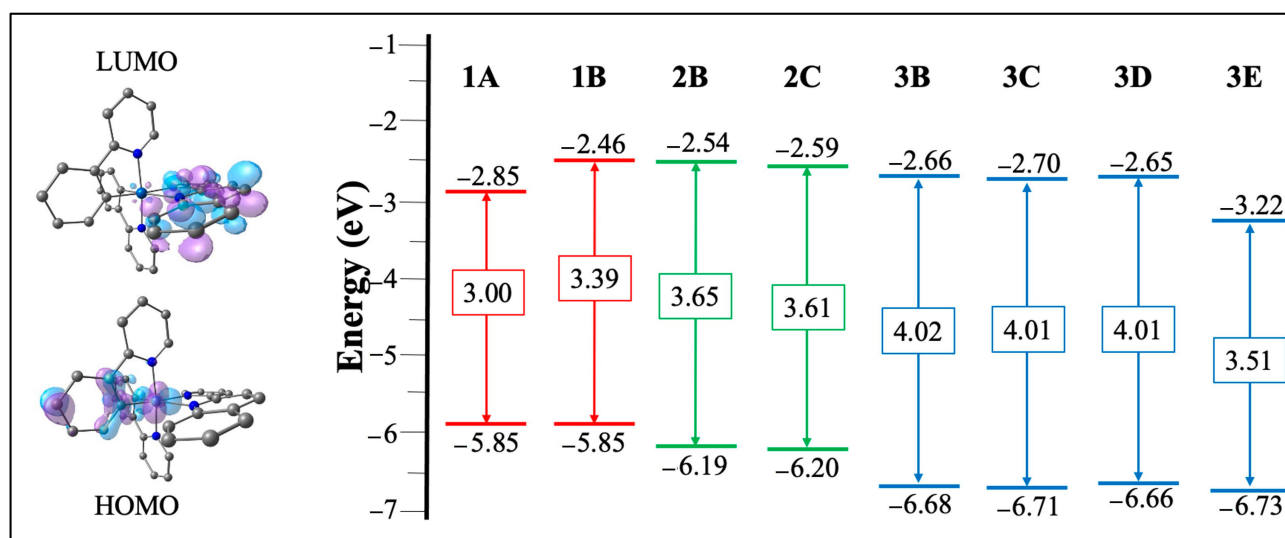


Figure 2. Molecular orbitals diagram for all complexes and HOMO–LUMO plots for **1A** as representative of all complexes (for the rest of the complexes, see Figures S1–S3).

The HOMO orbital is distributed between the d-orbital of the metal center (33–41%) and the phenyl ring orbitals of the C[^]N ligand (57–62%), and the LUMO orbital being exclusively on the N_N ligand (~95%) in all complexes. This electron density distribution agrees with the literature data for similar Ir(III) complexes [15,25,55].

Series **1** displays small values of Δ HL; **1A** = 3.00 eV and **1B** = 3.39 eV. With the increase of an aromatic ring fused in the framework of the **A** ancillary ligand, it is incrementing the π -accepting character of this ligand. The increment of conjugation in the ancillary ligands causes an enhancement of the electron withdrawing effect, therefore, the LUMO orbitals are stabilized, reducing the Δ HL of **1A** compared to **1B** [60,61]. Thus, since **1A** shows the

lowest Δ H_L of the complexes studied, the absorption and emission energy of this complex is expected to be the most red-shifted.

Series 2 has intermediate Δ H_L values; **2B** = 3.65 eV and **2C** = 3.61 eV. This variation, with respect to series 1, is mainly attributed to the energetic stabilization that the HOMO orbital undergoes due to the electron-withdrawing character of the fluorine atoms present in the C[^]N ligand [62–65]; therefore, series 2 is expected to present emissions in the green region. This trend has been observed in similar Ir(III) complexes, where the presence of the electron-withdrawing substituents present in the aromatic rings of the C[^]N ligands promote greater stabilization of the HOMO orbital, demonstrated, for example, by cyclic voltammetry studies, where the oxidation peak associated with the C[^]N ligand and the d orbitals of the metal is shifted to higher potentials, with respect to the oxidation of the analogous complexes with the C[^]N ligands without the electron withdrawing substituents [66].

Finally, the largest Δ H_L values are for the series 3; **3B** = 4.02 eV and **3C** = **3D** = 4.01 eV, except for **3E** = 3.51 eV. The introduction of the N onto the aromatic ring of the C[^]N ligand, plus the presence of the fluorine atoms, has a significant effect on the HOMO energy stabilization, [23] increased in the HOMO–LUMO energy gap compared to the complexes of the series 1 and 2, which probably will result in blue-shifted emissions. In the case of the **3E** complex, its Δ H_L is considerably reduced due to the stabilization of the LUMO by the presence of the E ligand, with high electron delocalization that increases their electron acceptor character, as has been described in analogous Ir(III) complexes with a 2,2'-biquinoline as N[^]N ancillary ligand [38,67].

3.3. Absorption Properties

The absorption properties were obtained in dichloromethane on the optimized ground state geometries, the analysis of the absorptions was focused on MLCT bands in the region between 320 to 440 nm and are listed in Table 2.

Table 2. Absorption properties calculated from TD-DFT approach, in dichloromethane as solvent. Determined at the B3LYP/6-31G(d)/LANL2DZ level of theory.

System	State	E _{abs} (λ _{abs})	f	Monoexcitations	Description
1A	S ₄	2.83 (437)	0.077	H-3→L (80%)	Ir(d) + C [^] N(π)→N [^] N(π*); ¹ MLCT/ ¹ LLCT
	S ₅	2.99 (414)	0.042	H→L + 1 (97%)	Ir(d) + C [^] N(π)→C [^] N(π*); ¹ MLCT/ ¹ ILCT
	S ₂	3.14 (394)	0.036	H→L + 1 (96%)	Ir(d) + C [^] N(π)→C [^] N(π*); ¹ MLCT/ ¹ ILCT
1B	S ₆	3.46 (358)	0.064	H-3→L (87%)	Ir(d) + C [^] N(π)→N [^] N(π*); ¹ MLCT/ ¹ LLCT
	S ₂	3.34 (371)	0.035	H→L + 1 (94%)	Ir(d) + C [^] N(π)→C [^] N(π*); ¹ MLCT/ ¹ ILCT
2B	S ₆	3.65 (440)	0.050	H-3→L (54%) H-4→L (18%)	Ir(d) + C [^] N(π)→N [^] N(π*); ¹ MLCT/ ¹ LLCT Ir(d) + C [^] N(π)→N [^] N(π*); ¹ MLCT/ ¹ LLCT
	S ₃	3.41 (363)	0.026	H→L + 2 (82%)	Ir(d) + C [^] N(π)→C [^] N(π*); ¹ MLCT/ ¹ ILCT
2C	S ₇	3.58 (346)	0.050	H-3→L (66%)	Ir(d) + C [^] N(π)→N [^] N(π*); ¹ MLCT/ ¹ LLCT
	3B	S ₂	3.66 (339)	0.023	H→L + 1 (81%)
S ₄		3.70 (335)	0.035	H-1→L (78%)	C [^] N(π)→N [^] N(π*); ¹ LLCT
3C	S ₃	3.63 (341)	0.041	H-2→L (67%)	Ir(d) + C [^] N(π) + N [^] N(π)→N [^] N(π*); ¹ MLCT/ ¹ LLCT/ ¹ ILCT
	S ₇	3.79 (327)	0.028	H→L + 2 (35%)	Ir(d) + C [^] N(π)→C [^] N(π*) + N [^] N(π*); ¹ MLCT/ ¹ LLCT/ ¹ ILCT
				H→L + 1 (24%)	Ir(d) + C [^] N(π)→N [^] N(π*); ¹ MLCT/ ¹ LLCT
H-1→L (14%)				C [^] N(π)→N [^] N(π*); ¹ LLCT	
3D	S ₃	3.66 (338)	0.054	H-1→L (88%)	C [^] N(π)→N [^] N(π*); ¹ LLCT
	S ₇	3.88 (319)	0.092	H-4→L (85%)	Ir(d) + C [^] N(π) + N [^] N(π)→N [^] N(π*); ¹ MLCT/ ¹ LLCT/ ¹ ILCT
3E	S ₃	3.16 (391)	0.048	H-2→L (45%) H-1→L (35%)	Ir(d) + C [^] N(π) + N [^] N(π)→N [^] N(π*); ¹ MLCT/ ¹ LLCT/ ¹ ILCT C [^] N(π)→N [^] N(π*); ¹ LLCT
	S ₇	3.60 (344)	0.048	H-5→L (48%) H-6→L (42%)	Ir(d) + N [^] N(π)→N [^] N(π*); ¹ MLCT/ ¹ LC N [^] N(π)→N [^] N(π*); ¹ LC

The lowest absorption bands of series **1** are found between 358 to 437 nm, involving HOMO (HOMO-3) \rightarrow LUMO (LUMO+1) orbitals. For series **2**, these absorption bands are located at slightly higher energies than series **1**, between 346 and 410 nm, which arises mainly from HOMO (HOMO-1, HOMO-3, HOMO-4) towards LUMO (LUMO+1, LUMO+2) orbitals. Finally, in series **3**, the absorption bands exhibit a considerable blue-shifting (319 to 391 nm) and two trends can be observed, namely, for **3B** and **3C** the lowest lying absorptions are attributed to the HOMO (HOMO-1, HOMO-2) \rightarrow LUMO (LUMO+1, LUMO+2) transitions, while **3D** and **3E** involves HOMO-1 to HOMO-6 \rightarrow LUMO orbitals. According to the analysis carried out on the compositions of the molecular orbitals, it is observed that, in all the complexes, the low-energy absorptions have mainly a mixed transition character $^1\text{MLCT}/^1\text{LLCT}/^1\text{ILCT}$ (ILCT: intraligand charge transfer); in the case of **3E**, this additionally presents a transition with a strong ^1LC (LC: ligand centered) character, centered on the ancillary ligand (2,2'-biquinoline, **E**).

In summary, we observe that the presence of the fluorine atoms in the C^N ligand (in series **2**), as well as the additional incorporation of the nitrogen atom in the C^N ligand skeleton (series **3**), has a significant influence in the blue-shift of the lowest absorption bands compared to series **1**, which allows the prediction that such complexes present the expected emission at a higher energy. On the other hand, the remarkable participation of MLCT in the region of interest could be indicative of an efficient intersystem crossing throughout the three series, which anticipates a good emission performance.

3.4. Emission Properties

The luminescent properties of the complexes in this study were determined based on the minimum energy structures of the lowest triplet excited states, obtained using the TD-DFT formalism. The main results are listed in Table 3.

Table 3. Excited states properties of the Ir(III) complexes studied calculated from TD-DFT approach.

Complexes	State	$\lambda_{\text{emi}}/\text{nm}$ (E_{emi}/eV)	Main Configuration	Character
1A	T ₁	701 (1.77)	L \rightarrow H (99%)	N ^N (π^*) \rightarrow Ir(d) + C ^N (π); $^3\text{MLCT}/^3\text{LLCT}$
1B	T ₁	599 (2.07)	L \rightarrow H (97%)	N ^N (π^*) \rightarrow Ir(d) + C ^N (π); $^3\text{MLCT}/^3\text{LLCT}$
2B	T ₂	547 (2.26)	L + 1 \rightarrow H (69%)	C ^N (π^*) \rightarrow Ir(d) + C ^N (π); $^3\text{MLCT}/^3\text{ILCT}$
2C	T ₂	548 (2.26)	L + 1 \rightarrow H (48%) L + 2 \rightarrow H (24%)	N ^N (π^*) + C ^N (π^*) \rightarrow Ir(d) + C ^N (π); $^3\text{MLCT}/^3\text{LLCT}/^3\text{LC}$ N ^N (π^*) + C ^N (π^*) \rightarrow Ir(d) + C ^N (π); $^3\text{MLCT}/^3\text{LLCT}/^3\text{LC}$
3B	T ₂	448 (2.76)	L \rightarrow H (79%)	N ^N (π^*) \rightarrow Ir(d) + C ^N (π); $^3\text{MLCT}/^3\text{LLCT}$
3C	T ₃	454 (2.73)	L \rightarrow H-1 (43%) L \rightarrow H (41%)	N ^N (π^*) \rightarrow Ir(d) + N ^N (π) + C ^N (π); $^3\text{MLCT}/^3\text{LLCT}/^3\text{LC}$ N ^N (π^*) \rightarrow Ir(d) + C ^N (π); $^3\text{MLCT}/^3\text{LLCT}$
3D	T ₂	440 (2.82)	L \rightarrow H (92%)	N ^N (π^*) \rightarrow Ir(d) + C ^N (π); $^3\text{MLCT}/^3\text{LLCT}$
3E	T ₂	574 (2.16)	L \rightarrow H-2 (26%) L \rightarrow H (19%) L \rightarrow H-1 (18%)	N ^N (π^*) \rightarrow Ir(d) + C ^N (π); $^3\text{MLCT}/^3\text{LLCT}$ N ^N (π^*) \rightarrow Ir(d) + C ^N (π); $^3\text{MLCT}/^3\text{LLCT}$ N ^N (π^*) \rightarrow Ir(d) + N ^N (π) + C ^N (π); $^3\text{MLCT}/^3\text{LLCT}/^3\text{LC}$

The obtained emission energies are 1.77 and 2.07 eV for complexes **1A** and **1B**, respectively, indicating that the increase in conjugation of the ancillary ligand **A** leads to a more red-shifted emission, in agreement with the HOMO–LUMO gap. In both complexes, the emitting state (T₁) has a mixed character of $^3\text{MLCT}/^3\text{LLCT}$ and arises from the LUMO \rightarrow HOMO transition, as can be noted in Figure 3 (see Supplementary Materials Figures S4–S6 for all complexes).

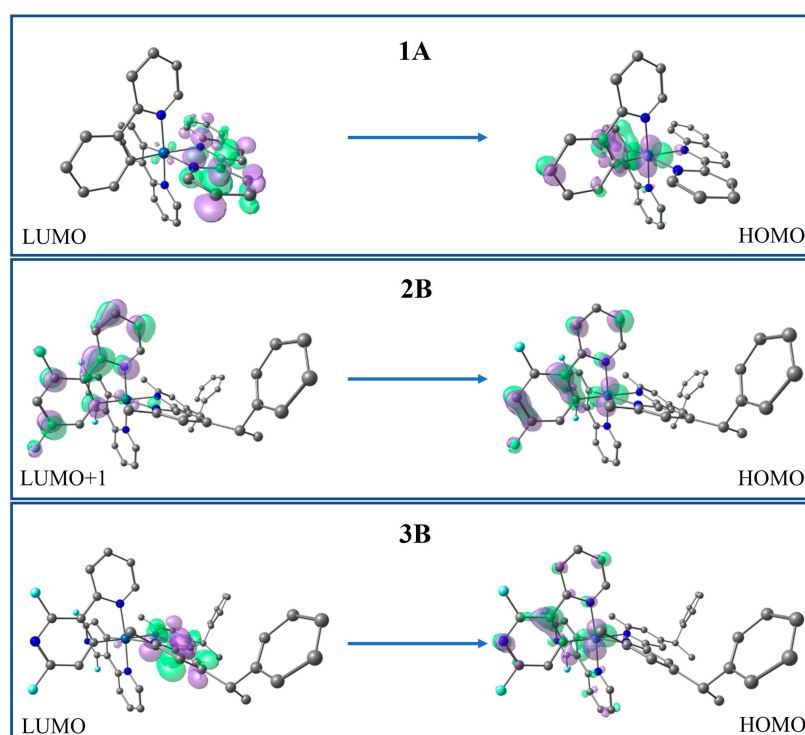


Figure 3. Radiative deactivation pathway of the triplet excited state of **1A**, **2B** and **3B**, as representative of each series (for the rest of the complexes, see Figures S4–S6).

In series **2**, it is observed that the fluorine atoms in the cyclometalating ligand cause a displaced emission at high energy in complexes **2B** and **2C** (~2.26 eV), compared to series **1**, as we expected, since this strategy has been widely used to favor blue-shifted emissions [64,65]. For both **2B** and **2C** the emitter state found corresponds to T_2 . The emission of **2B** originates from the LUMO→HOMO-1 transition with a ${}^3\text{MLCT}$ and ${}^3\text{ILCT}$ character, while, for **2C**, it is predominantly contributed to by the LUMO+1(LUMO+2)→HOMO transitions and its emissive state shows a mixed ${}^3\text{MLCT}/{}^3\text{LLCT}/{}^3\text{LC}$ character.

In series **3**, the addition of fluorine and nitrogen atoms to the C[∞]N ligand blue-shifts the emission further with respect to series **2**, i.e., the emission energies obtained were 2.76, 2.73 and 2.82 eV, for **3B**, **3C** and **3D**, respectively. The exception is **3E**, which displays a significantly lower emission energy compared to the rest of the complexes, shifting its emission to the yellow region of the visible spectrum; this behavior is attributed to the increased conjugation of the E ancillary ligand, which stabilizes the energy of LUMO, as commented previously. The emitting state for **3B**, **3D** and **3E** corresponds to T_2 , while for **3C**, it is T_3 . Two trends are observed in the nature of the emitting excited state: the complexes **3B** and **3D** can be described with ${}^3\text{MLCT}/{}^3\text{LLCT}$ mixed characters and for **3C** and **3E**, a mixed ${}^3\text{MLCT}/{}^3\text{LLCT}/{}^3\text{LC}$ character. In all these complexes, the deactivation pathway originates from LUMO towards HOMO (HOMO-1, HOMO-2).

Regarding the emission energies found, the designed complexes showed a significant emission color tuning from deep red to blue, i.e., the complexes **1A** and **1B** could be exhibiting red emissions; for **2B**, **2C** and **3E** the emissions ranged at green, and finally, emissions at blue should be displayed for **3B**, **3C** and **3D**.

3.5. Phosphorescence Quantum Efficiency

From the photoluminescence quantum yield (Φ) we can quantify the efficiency of the emission process. The Φ is determined by the competition between the radiative rate constant (k_r) and the non-radiative rate constant (k_{nr}), according to the following relation: [68,69]

$$\Phi = k_r / (k_r + k_{nr}) \quad (1)$$

The k_r is usually expressed as: [63]

$$k_r = \gamma(\langle \Psi_{S_1} | H_{SO} | \Psi_{T_n} \rangle^2 \mu_{S_1}^2) / (\Delta E(S_1 - T_n)^2); \text{ with } \gamma = (16\pi^3 10^6 n^3 E_{emi}^3) / (3h\epsilon_0) \quad (2)$$

where $\langle \Psi_{S_1} | H_{SO} | \Psi_{T_n} \rangle$ is the spin-orbit coupling (SOC) matrix element between the S_1 state and the emitting state (T_1 , T_2 or T_3), μ_{S_1} is the transition electronic dipole moment in $S_0 \rightarrow S_1$ transition, $\Delta E(S_1 - T_n)$ is the energy gap between the S_1 state and the emitting triplet state, and n , E_{emi} , h and ϵ_0 are the refractive index of the medium, emission energy, Planck's constant, and the permittivity in vacuum, respectively. This expression is applicable to coordination compounds with a heavy metal center since the radiative rate is directly proportional to the SOC matrix element related to the emitting triplet and singlet states, and inversely proportional to the degree of mix between them ($\Delta E(S_1 - T_n)$). In these type of complexes, large intersystem crossing rates (ISC) predominate, so the fluorescence rate can be considered null, as well as some non-radiative pathways (inverse ISC, internal conversion, conversion from MLCT to MC) [70].

The SOC effects can be elucidated from the metal contribution in the emitting state (%³MLCT), which were calculated from the sum of the ³MLCT contributions from each monoexcitation (according to their respective orbitals involved), considering the corresponding configuration coefficient, as has been reported in the literature [71,72]. The results are summarized in Table 4.

Table 4. Metal–ligand charge transfer character (³MLCT, %), transition electric dipole moment (μ_{S_1} , D) and energy gaps between the S_1 and T_n states ($\Delta E(S_1 - T_n)$, eV) of studied complexes.

Complexes	% ³ MLCT	μ_{S_1}	$\Delta E(S_1 - T_n)$
1A	32.4	0.61	0.043
1B	33.2	1.26	0.057
2B	19.6	1.22	0.110
2C	20.7	1.11	0.144
3B	27.6	0.60	0.020
3C	23.4	1.00	0.330
3D	30.8	0.14	0.009
3E	18.2	0.94	0.275

According to Equation (2), higher values of %³MLCT and μ_{S_1} increase the k_r value and, conversely, higher values of $\Delta E(S_1 - T_n)$ decrease the k_r . We observe that, in all complexes, the %³MLCT is high enough, therefore, k_r is favored in all cases. However, the higher values are obtained for the complexes of series **1** and series **3** (except for **3E**), which suggests that the %³MLCT is affected by the different C^N ligands used. Interestingly, these complexes showed structural changes in the excited state (T_1 , T_2 or T_3) that would favor the metal–ligand interaction, namely, a shortening of the length of Ir–N_{N'} ligand bonds (Ir–N₂ and Ir–N₃).

For μ_{S_1} , the variation of the C^N and N^N ligands do not show a clear trend. The largest values are shown by **1B**, **2B**, **2C**, and **3C** (between 1.26 to 1.00 D), so higher k_r values are expected in these complexes.

On the other hand, a minimal difference between the S_1 and the emitting state, $\Delta E(S_1 - T_n)$, is favorable for enhancing the intersystem crossing (ISC) rate, implying an increase in k_r . The results show significantly lower values for complexes **3D**, **3B**, **1A**, and **1B**, and precisely, in these complexes, the highest values of %³MLCT (~27% to 33%) are observed, as expected since a high SOC (%³MLTC) promotes an effective ISC.

In summary, considering all the parameters that determine the k_r value, it is observed that the **1A**, **1B**, **2B**, **2C**, **3B**, and **3D** complexes would present characteristics that favor the radiative deactivation processes.

Equation (1) shows that another determining factor in the efficiency of the emission process corresponds to the k_{nr} . The population of metal-centered (³MC, d-d*) triplet excited states is one of the most important deactivation pathways of the phosphorescence, namely,

the $^3\text{MLCT}$ ($\pi\text{-}\pi^*$) excited state can be rapidly converted to a short-lived ^3MC ($d\text{-}d^*$) state, from which no emission occurs; to avoid this situation, a splitting in energy is required between the ^3MC and $^3\text{MLCT}$ states [25,73,74].

The metal–ligand bond lengths and bond angles in ^3MC states are listed in Table S5 (see Supplementary Materials), along with the spin density distributions determined for the ^3MC state (see Figure S7) where the metal-centered character is observed. The results show that, in almost all complexes, the main structural change in the ^3MC states correspond to the distance between the metal and the N atoms located in the axial position (Ir–N₁/Ir–N₄), which increase up to 0.6 Å, with respect to ground state. However, complexes **1A** and **3C** showed a relatively small structural distortion between the ^3MC and S_0 states, which would explain the lower energies obtained for these ^3MC states.

In general, it is observed that, in almost all complexes, the relative energy position of the ^3MC state lies above the emitting triplet state $^3\text{MLCT}$, except for complexes **3B** and **3C**, as shown in Figure 4. This is explained due to the electron withdrawing character of the cyclometalating ligand (**3**), therefore, it strongly influences the increase in the energy of the $^3\text{MLCT}$ excited state, which, in some cases, causes it to exceed the energy of the ^3MC state. High energies of the $^3\text{MLCT}$ excited states have been identified for analogous Ir(III) complexes with this cyclometalating ligand [75–78]. This effect is almost experienced by **3D** ($^3\text{MLCT}$ energy close to ^3MC energy) and, in the case of **3E**, the effect is not observed since the E ligand (electron withdrawing by resonance) compensates for the effect of the cyclometalating ligand.

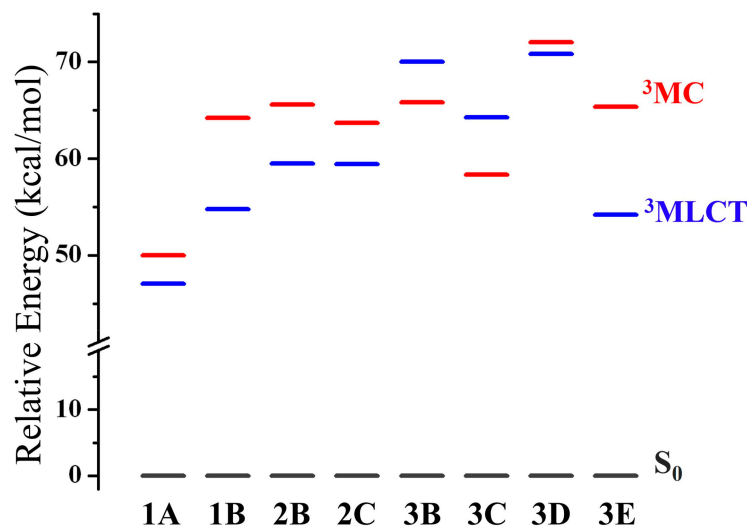


Figure 4. Energy level diagram of all complexes under study of $^3\text{MLCT}$, ^3MC and S_0 states (normalized).

With regard to the behavior of the **3B** and **3D** complexes, a similar tendency should be expected, since the aliphatic bonds and substituents in the 4 and 4' positions should not influence the electronic properties. However, to elucidate why, in one case, the ^3MC (**3B**) is stabilized and in the other, the $^3\text{MLCT}$ (**3D**) is destabilized, we calculated the root-mean-square deviation (RMSD), determining the difference between two sets of the coordinate values, in this case between the $^3\text{MLCT}$ and ^3MC excited states (see Supplementary Materials Figure S8). For the **3B** complex, a higher value (0.668 Å) was found compared to **3D** (0.494 Å), which would explain the higher energy gap in **3B**, probably due to the high mobility of the substituents in the 4,4' positions, yielding a ^3MC state that is more stabilized. Whereas in **3D**, the lower value of RMSD indicates less distortion (in fact, both states have very similar energies), where the $^3\text{MLCT}$ state is most stable.

The computed adiabatic energy differences between the ^3MC and $^3\text{MLCT}$ ($\Delta E(^3\text{MC}\text{-}^3\text{MLCT})$) are 0.13, 0.41, 0.26, 0.19, -0.18 , -0.26 , 0.05, and 0.48 eV for **1A**, **1B**, **2B**, **2C**, **3B**, **3C**, **3D**, and **3E**, respectively. High $\Delta E(^3\text{MC}\text{-}^3\text{MLCT})$ values of iTMCs, in the range of 0.26–0.60 eV, have shown high electroluminescent performance in LEC devices [79]. Consequently, the

complexes **1B**, **2B**, and **3E** would lead to a lower k_{nr} and would present a high performance in their application in LEC. While the probability of populating the 3MC states increases in complexes **1A**, **2C**, and **3D**, which would result in a more favored k_{nr} , as the emission of **3B** and **3C** comes from very high 3MLCT states (blue-shifted emission), [21] the conversion from the emitting state to the 3MC state is easily completed, thereby increasing the probability of non-radiative decay to the ground state and consequently, a significantly larger k_{nr} is obtained. Note that the **3D** blue emitting state also displays a high 3MLCT state.

3.6. Charge Transfer Properties: IP and EA

The good performance of LEC devices is determined by the appropriate injection and transfer of holes and electrons, which can be evaluated by the ionization potential (IP), electron affinity (EA), and reorganization energy (λ). The IP and EA are obtained as: [49–51]

$$IP = E_{N-1} - E_N \quad (3)$$

$$EA = E_N - E_{N+1} \quad (4)$$

where E_N , E_{N+1} , E_{N-1} are the total energies of the molecular system in its ground state, with one electron more and one electron less, respectively. Small IP values indicate easy hole injection from the anode to the HOMO of the iTMC, and large EA values can be related to a favored electron injection from the cathode to the LUMO of the iTMC [25,80,81]. As shown in Table 5, the IP values gradually increase in the following order: Series **1** < Series **2** < Series **3**, which is consistent with the HOMO energy levels (see Section 3.2). Therefore, the C \bar{N} ligand largely determines the HOMO level, establishing that ligand **1** causes a lower hole injection energy barrier compared to ligands **2** and **3**. In this sense, series **1** could display the best hole injection performance.

Table 5. The Ionization potential (IP , eV), electron affinities (EA , eV), hole/electron reorganization energy (λ_h/λ_e , eV) and $\Delta\lambda$ (eV).

Complexes	IP	EA	λ_h	λ_e	$\Delta\lambda = \lambda_e - \lambda_h$
1A	5.85	2.83	0.19	0.32	0.13
1B	5.85	2.42	0.18	0.45	0.27
2B	6.20	2.50	0.16	0.46	0.30
2C	6.21	2.55	0.15	0.33	0.18
3B	6.70	2.63	0.12	0.44	0.32
3C	6.72	2.65	0.12	0.33	0.21
3D	6.67	2.59	0.13	0.40	0.27
3E	6.75	3.21	0.12	0.32	0.20

Related to the EA , the highest values are found in **1A** and **3E**, showing agreement with the lowest energies of the LUMO levels, according to the electron acceptor character of the N \bar{N} ligand. Consequently, these three complexes will have an enhanced electron injection ability compared to other complexes.

On the other hand, the reorganization energy can be used to estimate the charge transport rate and balance between holes (λ_h) and electrons (λ_e) according to the following expression: [23,82,83]

$$\lambda_h = IP - HEP \quad (5)$$

$$\lambda_e = EEP - EA \quad (6)$$

HEP (EEP) is the hole (electron) extraction potential and is determined as the vertical energy difference between the ground state and the relaxed state with one electron less (more), using the geometry with one electron less (more), respectively. Generally, a low reorganization energy (λ_h , λ_e) is necessary for an efficient charge transport process and in this respect, the full series **3** appears to be more efficient in the hole transport ($\lambda_h = 0.12$ to 0.13 eV) while complexes **1A**, **2C**, **3C**, and **3E** showed greater efficiency in electron transport. However, in all complexes, the hole transport performance is favored over the electron

transport ability, due to the higher values obtained of λ_e (0.32 to 0.46 eV), with respect to λ_h (0.12 to 0.19 eV).

In addition, we determined the difference between λ_h and λ_e , and it was observed that the complexes **1A**, **2C**, **3C**, and **3E** showed less discrepancy ($\Delta\lambda < 0.21$), indicating that the balance of electron and hole transfer could be easily achieved in the emitting layer of the LEC devices.

3.7. RGB Systems to Produce White LECs

According to the emission energies determined for each complex studied, in Table 6, in the first line, the complexes were organized from the reddest emitter to the bluest emitter, from left to right, respectively. It can be observed that this order differs with respect to the original tendency designed, since it was expected that the type of cyclometalating ligand chosen was the main factor determining the emission energy. In this sense, the **3E** complex is out of the original tendency since their ancillary ligands promote a strong stabilization of LUMO, which shifted their emissions at lower energies. Then, in the following lines of the table, an arbitrary qualification has been used for each studied complex with respect to the values of k_r , k_{nr} , IP , EA , and $\Delta\lambda$. This qualification arises from the parameters determined in Sections 3.5 and 3.6, based on the minimum and maximum values determined, and also considering key values from the literature. Then, the +++ symbol is assigned to a very favourable value, ++ to a favourable value, and + is slightly favourable. In the case of k_{nr} , a 0 value is added to qualify the parameter with an unfavourable value. The extension of the criteria assigned can be observed in the Supporting Information.

Table 6. Analyzed photophysics and charge transport parameters to determine the best RGB systems.

Complexes	1A	1B	3E	2C	2B	3C	3B	3D
Color	Red	Red	Green	Green	Green	Blue	Blue	Blue
λ_{em}/nm	701	599	574	548	547	454	448	440
k_r	++	+++	+	++	++	+	+++	++
k_{nr}	+	++	++	+	++	0	0	+
IP	+++	+++	+	++	++	+	+	+
EA	+++	+	+++	+	+	++	++	++
$\Delta\lambda$	+++	++	+++	+++	+	+++	+	++

By the analysis of k_r and k_{nr} kinetic parameters, that describe the efficiency of the intrinsic radiative process of the complex, it is observed that, for red emitter complexes, the best combination of these parameters is obtained in complex **1B**, therefore, this is the best candidate to be a good red emitter in an RGB system. Then, if IP , EA , and $\Delta\lambda$ parameters are considered, **1A** could be an appropriate red emitter. Next, in terms of the evaluation for the green emitter complexes, the best performance in the kinetic parameters of the phosphorescent processes is found for **2B**, therefore being the best candidate as a green emitter. Then, if the charge transport and injection parameters are considered, plus its balance, **3E** and finally **2C** could be proposed.

Finally, for the emitter complexes in the blue range, only **3D** could act as an appropriate emitter for an RGB system, since the other blue complexes have a very unfavourable k_{nr} . This behaviour in **3C** and **3B** is due to the higher energy of the 3MLCT states with respect to 3MC , promoting this 3MC state as the phosphorescence deactivator, which is known to prefer non-radiative paths.

Consequently, according to this analysis, a proposal for dual host–guest system with blue and red emitters to produce white LECs could be obtained by mixing **3D–1B**, as well as **3D–1A**. In the case of an RGB system, the proposal would be to assemble the **3D–2B–1B** complexes.

4. Conclusions

A detailed investigation is reported on the geometrical and electronic structures, emission properties, charge injection/transport abilities, and phosphorescence efficiency of eight new Ir(III) complexes (classified into 3 series) using DFT and TD-DFT methods.

The designed complexes showed a significant emission color tuning from deep red to blue, with emissions ranging from 440 to 701 nm. The results showed that the Ir-N[^]N ligand bond lengths are shortened for complexes of series 1 and 3, which has a direct impact on the metal–ligand interaction, leading to more involvement of the metal in the triplet excited state (³MLCT). The analysis of quantum efficiency showed that the 1A, 1B, 2B, 2C, 3B, and 3D complexes would present characteristics that favor the radiative deactivation processes, while 1B, 2B, and 3E complexes would lead to a lower k_{nr} and would present a high performance in their application in LEC. In relation to transport and injection parameters, the complexes with the best balance between hole and electron injection are 1A, 2C, 3C, and 3E ($\Delta\lambda < 0.21$), however, the full Series 3 stands out for being more efficient in the hole transport, and 1A, 2C, 3C, and 3E, for presenting greater efficiency in the transport of electrons. Finally, we have proposed a host–guest dual system using a mix of 3D and 1B, and also an RGB system based on 3D–2B–1B, to produce white LECs.

With this family of complexes, corresponding to newly designed structures based on a mix of C[^]N and N[^]N ligands, commercially available and/or easy to synthesize, an important contribution of new Ir-iTMCs is provided from a theoretical approach, which is totally experimentally viable.

Supplementary Materials: The following supporting information can be downloaded at: <https://www.mdpi.com/article/10.3390/molecules27092623/s1>. Section S1. Benchmark study with other DFT functionals; Table S1. Absorption and Emission wavelengths from ground and triplet excited states, respectively, for [Ir(ppy)₂(bpy)]⁺ (in dichloromethane); Section S2. Geometry parameters of the ground states and the triplet states; Table S2. Optimized geometric parameters of all complexes under study in the S₀ and T₁ states, determined at the B3LYP/6-31G(d)-LANL2DZ level of theory; Section S3. Energies of the molecular orbitals from HOMO-2 to LUMO+2, in the ground state; Table S3. Energy of frontier molecular orbitals (eV) and ΔH_L of the ground state (S₀); Section S4. Contribution to molecular orbitals from HOMO-2 to LUMO+2, in the ground state; Table S4. Contribution to molecular orbitals (%) of all complexes calculated from HOMO-2 to LUMO+2 in the ground state (S₀); Section S5. Surface orbitals from HOMO and LUMO in the ground state; Figure S1. Surface of frontier molecular orbitals HOMO and LUMO (S₀) of series 1; Figure S2. Surface of frontier molecular orbitals HOMO and LUMO (S₀) of series 2; Figure S3. Surface of frontier molecular orbitals HOMO and LUMO (S₀) of series 3; Section S6. Molecular orbitals of the triplet excited state; Figure S4. Frontier molecular orbitals involved in the radiative deactivation of the lowest-lying triplet excited state of series 1; Figure S5. Frontier molecular orbitals involved in the radiative deactivation of the lowest-lying triplet excited state of series 2; Figure S6. Frontier molecular orbitals involved in the radiative deactivation of the lowest-lying triplet excited state of series 3; S7. Geometry parameters of ³MC state; Table S5. Selected geometric parameters of all complexes under study in the ³MC state, determined at the B3LYP/6-31G(d)-LANL2DZ level of theory; Section S8. Spin density of ³MC state; Figure S7. Spin density distribution in the optimized ³MC state for representative complexes; Section S9. Root-mean-square deviation (RMSD) between the ³MLCT and ³MC states; Figure S8. Superimposed structures of the ³MLCT states (blue) and ³MC states (orange) for 3B and 3D, and their RMSD values; Section S10. Qualification scales of k_r , k_{nr} , IP , EA and $\Delta\lambda$ to choose RGB systems; Table S6. Photophysics and charge transport parameters to determine the best RGB systems; Table S7. Building scales to quantify the photophysics and charge transport parameters to determine the best RGB systems.

Author Contributions: Conceptualization, M.S.-N. and P.D.; methodology, M.S.-N. and P.D.; software, M.S.-N. and B.B.; validation, M.S.-N., B.B. and P.D.; formal analysis, M.S.-N., B.B., D.Z., L.R. and P.D.; investigation, M.S.-N., B.B., D.Z., L.R. and P.D.; resources, M.S.-N. and P.D.; data curation, M.S.-N., F.S., L.R. and D.Z.; writing—original draft preparation, M.S.-N., B.B., F.S. and P.D.; writing—review and editing, B.B., F.S., D.Z., L.R. and P.D.; visualization, M.S.-N. and F.S.; supervision, M.S.-N. and P.D.; project administration, M.S.-N. and P.D. All authors have read and agreed to the published version of the manuscript.

Funding: This research was funded by Agencia Nacional de Investigación y Desarrollo: 3170663, 1201173 and IDP210010 projects; Federico Santa María Technical University: PI_M_2020_31 USM project. The APC was funded by Agencia Nacional de Investigación y Desarrollo: 1201173 project.

Institutional Review Board Statement: Not applicable.

Informed Consent Statement: Not applicable.

Acknowledgments: F.S. acknowledge to ANID Scholarship. This research was supported by the high-performance computing system of PIDi-UTEM (SCC-PIDi-UTEM FONDEQUIP-EQM180180).

Conflicts of Interest: There are no conflicts to declare.

Sample Availability: Samples of the compounds are not available from the authors.

References

1. Graham-Rowe, D. Electronic Paper Rewrites the Rulebook for Displays. *Nat. Photonics* **2007**, *1*, 248–251. [[CrossRef](#)]
2. Fresta, E.; Costa, R.D. Beyond Traditional Light-Emitting Electrochemical Cells—a Review of New Device Designs and Emitters. *J. Mater. Chem. C* **2017**, *5*, 5643–5675. [[CrossRef](#)]
3. Koizumi, H. Development and Practical Applications of Blue Light-Emitting Diodes. *Engineering* **2015**, *1*, 167–168. [[CrossRef](#)]
4. Burroughes, J.H.; Bradley, D.D.C.; Brown, A.R.; Marks, R.N.; Mackay, K.; Friend, R.H.; Burns, P.L.; Holmes, A.B. Light-Emitting Diodes Based on Conjugated Polymers. *Nature* **1990**, *347*, 539–541. [[CrossRef](#)]
5. Tordera, D.; Meier, S.; Lenes, M.; Costa, R.D.; Ortí, E.; Sarfert, W.; Bolink, H.J. Simple, Fast, Bright, and Stable Light Sources. *Adv. Mater.* **2012**, *24*, 897–900. [[CrossRef](#)]
6. Adachi, C.; Baldo, M.A.; Thompson, M.E.; Forrest, S.R. Nearly 100% Internal Phosphorescence Efficiency in an Organic Light Emitting Device. *J. Appl. Phys.* **2001**, *90*, 5048–5051. [[CrossRef](#)]
7. Farinola, G.M.; Ragni, R. Electroluminescent Materials for White Organic Light Emitting Diodes. *Chem. Soc. Rev.* **2011**, *40*, 3467–3482. [[CrossRef](#)]
8. Gets, D.; Alahbakhshi, M.; Mishra, A.; Haroldson, R.; Papadimitratos, A.; Ishteev, A.; Saranin, D.; Anoshkin, S.; Pushkarev, A.; Danilovskiy, E.; et al. Reconfigurable Perovskite LEC: Effects of Ionic Additives and Dual Function Devices. *Adv. Opt. Mater.* **2021**, *9*, 2001715. [[CrossRef](#)]
9. He, L.; Wang, X.; Duan, L. Enhancing the Overall Performances of Blue Light-Emitting Electrochemical Cells by Using an Electron-Injecting/Transporting Ionic Additive. *ACS Appl. Mater. Interfaces* **2018**, *10*, 11801–11809. [[CrossRef](#)]
10. Van Reenen, S.; Matyba, P.; Dzwilewski, A.; Janssen, R.A.J.; Edman, L.; Kemerink, M. A Unifying Model for the Operation of Light-Emitting Electrochemical Cells. *J. Am. Chem. Soc.* **2010**, *132*, 13776–13781. [[CrossRef](#)]
11. Hu, T.; He, L.; Duan, L.; Qiu, Y. Solid-State Light-Emitting Electrochemical Cells Based on Ionic Iridium(III) Complexes. *J. Mater. Chem.* **2012**, *22*, 4206–4215. [[CrossRef](#)]
12. Kong, S.H.; Lee, J.I.; Kim, S.; Kang, M.S. Light-Emitting Devices Based on Electrochemiluminescence: Comparison to Traditional Light-Emitting Electrochemical Cells. *ACS Photonics* **2018**, *5*, 267–277. [[CrossRef](#)]
13. Frohleiks, J.; Wepfer, S.; Bacher, G.; Nannen, E. Realization of Red Iridium-Based Ionic Transition Metal Complex Light-Emitting Electrochemical Cells (ITMC-LECs) by Interface-Induced Color Shift. *ACS Appl. Mater. Interfaces* **2019**, *11*, 22612–22620. [[CrossRef](#)] [[PubMed](#)]
14. Lowry, M.S.; Bernhard, S. Synthetically Tailored Excited States: Phosphorescent, Cyclometalated Iridium(III) Complexes and Their Applications. *Chem.-A Eur. J.* **2006**, *12*, 7970–7977. [[CrossRef](#)] [[PubMed](#)]
15. Martínez-Alonso, M.; Cerdá, J.; Momblona, C.; Pertegás, A.; Junquera-Hernández, J.M.; Heras, A.; Rodríguez, A.M.; Espino, G.; Bolink, H.; Ortí, E. Highly Stable and Efficient Light-Emitting Electrochemical Cells Based on Cationic Iridium Complexes Bearing Arylazole Ancillary Ligands. *Inorg. Chem.* **2017**, *56*, 10298–10310. [[CrossRef](#)]
16. Meier, S.B.; Tordera, D.; Pertegás, A.; Roldán-Carmona, C.; Ortí, E.; Bolink, H.J. Light-Emitting Electrochemical Cells: Recent Progress and Future Prospects. *Mater. Today* **2014**, *17*, 217–223. [[CrossRef](#)]
17. Bai, R.; Meng, X.; Wang, X.; He, L. Blue-Emitting Iridium(III) Complexes for Light-Emitting Electrochemical Cells: Advances, Challenges, and Future Prospects. *Adv. Funct. Mater.* **2020**, *30*, 1907169. [[CrossRef](#)]
18. Henwood, A.F.; Zysman-Colman, E. Luminescent Iridium Complexes Used in Light-Emitting Electrochemical Cells (LEECs). *Top. Curr. Chem.* **2016**, *374*, 1–41. [[CrossRef](#)]
19. Costa, R.D.; Ortí, E.; Bolink, H.J.; Graber, S.; Schaffner, S.; Neuburger, M.; Housecroft, C.E.; Constable, E.C. Archetype Cationic Iridium Complexes and Their Use in Solid-State Light-Emitting Electrochemical Cells. *Adv. Funct. Mater.* **2009**, *19*, 3456–3463. [[CrossRef](#)]
20. Housecroft, C.E.; Constable, E.C. Over the LEC Rainbow: Colour and Stability Tuning of Cyclometalated Iridium(III) Complexes in Light-Emitting Electrochemical Cells. *Coord. Chem. Rev.* **2017**, *350*, 155–177. [[CrossRef](#)]
21. Costa, R.D.; Monti, F.; Accorsi, G.; Barbieri, A.; Bolink, H.J.; Ortí, E.; Armaroli, N. Photophysical Properties of Charged Cyclometalated Ir(III) Complexes: A Joint Theoretical and Experimental Study. *Inorg. Chem.* **2011**, *50*, 7229–7238. [[CrossRef](#)] [[PubMed](#)]
22. Xu, Q.L.; Wang, C.C.; Li, T.Y.; Teng, M.Y.; Zhang, S.; Jing, Y.M.; Yang, X.; Li, W.N.; Lin, C.; Zheng, Y.X.; et al. Syntheses, Photoluminescence, and Electroluminescence of a Series of Iridium Complexes with Trifluoromethyl-Substituted 2-Phenylpyridine as the Main Ligands and Tetraphenylimidodiphosphinate as the Ancillary Ligand. *Inorg. Chem.* **2013**, *52*, 4916–4925. [[CrossRef](#)] [[PubMed](#)]

23. Cortés-Arriagada, D.; Sanhueza, L.; González, I.; Dreyse, P.; Toro-Labbé, A. About the Electronic and Photophysical Properties of Iridium(III)-Pyrazino[2,3-f][1,10]-Phenanthroline Based Complexes for Use in Electroluminescent Devices. *Phys. Chem. Chem. Phys.* **2015**, *18*, 726–734. [[CrossRef](#)] [[PubMed](#)]
24. Zeng, Q.; Li, F.; Chen, Z.; Yang, K.; Liu, Y.; Guo, T.; Shan, G.G.; Su, Z. Rational Design of Efficient Organometallic Ir(III) Complexes for High-Performance, Flexible, Monochromatic, and White Light-Emitting Electrochemical Cells. *ACS Appl. Mater. Interfaces* **2020**, *12*, 4649–4658. [[CrossRef](#)]
25. Dreyse, P.; Santander-Nelli, M.; Zambrano, D.; Rosales, L.; Sanhueza, L. Electron-Donor Substituents on the Dppz-Based Ligands to Control Luminescence from Dark to Bright Emissive State in Ir(III) Complexes. *Int. J. Quantum Chem.* **2020**, *120*, e26167. [[CrossRef](#)]
26. Ladouceur, S.; Zysman-Colman, E. A Comprehensive Survey of Cationic Iridium(III) Complexes Bearing Nontraditional Ligand Chelation Motifs. *Eur. J. Inorg. Chem.* **2013**, *2013*, 2985–3007. [[CrossRef](#)]
27. González, I.; Dreyse, P.; Cortés-Arriagada, D.; Sundararajan, M.; Morgado, C.; Brito, I.; Roldán-Carmona, C.; Bolink, H.J.; Loeb, B. A Comparative Study of Ir(III) Complexes with Pyrazino[2,3-f][1,10]Phenanthroline and Pyrazino[2,3-f][4,7]Phenanthroline Ligands in Light-Emitting Electrochemical Cells (LECs). *Dalt. Trans.* **2015**, *44*, 14771–14781. [[CrossRef](#)]
28. Chen, H.F.; Wong, K.T.; Liu, Y.H.; Wang, Y.; Cheng, Y.M.; Chung, M.W.; Chou, P.T.; Su, H.C. Bis(Diphenylamino)-9,9'-Spirobifluorene Functionalized Ir(III) Complex: A Conceptual Design En Route to a Three-in-One System Possessing Emitting Core and Electron and Hole Transport Peripherals. *J. Mater. Chem.* **2011**, *21*, 768–774. [[CrossRef](#)]
29. Ertl, C.D.; Momblona, C.; Pertegás, A.; Junquera-Hernández, J.M.; La-Placa, M.G.; Prescimone, A.; Ortí, E.; Housecroft, C.E.; Constable, E.C.; Bolink, H.J. Highly Stable Red-Light-Emitting Electrochemical Cells. *J. Am. Chem. Soc.* **2017**, *139*, 3237–3248. [[CrossRef](#)]
30. Verboven, I.; Deferme, W. Printing of Flexible Light Emitting Devices: A Review on Different Technologies and Devices, Printing Technologies and State-of-the-Art Applications and Future Prospects. *Prog. Mater. Sci.* **2021**, *118*, 100760. [[CrossRef](#)]
31. Pashaei, B.; Karimi, S.; Shahroosvand, H.; Pilkington, M. Molecularly Engineered Near-Infrared Light-Emitting Electrochemical Cells. *Adv. Funct. Mater.* **2020**, *30*, 1908103. [[CrossRef](#)]
32. Uchida, S.; Nishikitani, Y. Exciplex Emission in Light-Emitting Electrochemical Cells and Light Outcoupling Methods for More Efficient LEC Devices. *Adv. Funct. Mater.* **2020**, *30*, 1907309. [[CrossRef](#)]
33. Youssef, K.; Li, Y.; O'Keefe, S.; Li, L.; Pei, Q. Fundamentals of Materials Selection for Light-Emitting Electrochemical Cells. *Adv. Funct. Mater.* **2020**, *30*, 1909102. [[CrossRef](#)]
34. Sarma, M.; Wong, K.T. Development of Materials for Blue Organic Light Emitting Devices. *Chem. Rec.* **2019**, *19*, 1667–1692. [[CrossRef](#)]
35. Ho, C.L.; Wong, W.Y.; Wang, Q.; Ma, D.; Wang, L.; Lin, Z. A Multifunctional Iridium-Carbazolyl Orange Phosphor for High-Performance Two-Element WOLED Exploiting Exciton-Managed Fluorescence/Phosphorescence. *Adv. Funct. Mater.* **2008**, *18*, 928–937. [[CrossRef](#)]
36. Su, H.C.; Chen, H.F.; Fang, F.C.; Liu, C.C.; Wu, C.C.; Wong, K.T.; Liu, Y.H.; Peng, S.M. Solid-State White Light-Emitting Electrochemical Cells Using Iridium-Based Cationic Transition Metal Complexes. *J. Am. Chem. Soc.* **2008**, *130*, 3413–3419. [[CrossRef](#)]
37. He, L.; Qiao, J.; Duan, L.; Dong, G.; Zhang, D.; Wang, L.; Qiu, Y. Toward Highly Efficient Solid-State White Light-Emitting Electrochemical Cells: Blue-Green to Red Emitting Cationic Iridium Complexes with Imidazole-Type Ancillary Ligands. *Adv. Funct. Mater.* **2009**, *19*, 2950–2960. [[CrossRef](#)]
38. Su, H.C.; Chen, H.F.; Shen, Y.C.; Liao, C.T.; Wong, K.T. Highly Efficient Double-Doped Solid-State White Light-Emitting Electrochemical Cells. *J. Mater. Chem.* **2011**, *21*, 9653–9660. [[CrossRef](#)]
39. Hu, T.; Duan, L.; Qiao, J.; He, L.; Zhang, D.; Wang, L.; Qiu, Y. Efficient Doped Red Light-Emitting Electrochemical Cells Based on Cationic Iridium Complexes. *Synth. Met.* **2013**, *163*, 33–37. [[CrossRef](#)]
40. Zeng, Q.; Li, F.; Guo, T.; Shan, G.; Su, Z. Synthesis of Red-Emitting Cationic Ir (III) Complex and Its Application in White Light-Emitting Electrochemical Cells. *Org. Electron.* **2017**, *42*, 303–308. [[CrossRef](#)]
41. Becke, A.D. Density-Functional Exchange-Energy Approximation with Correct Asymptotic Behavior. *Phys. Rev. A* **1988**, *38*, 3098–3100. [[CrossRef](#)]
42. Lee, C.; Yang, W.; Parr, R.G. Development of the Colle-Salvetti Correlation-Energy Formula into a Functional of the Electron Density. *Phys. Rev. B* **1988**, *37*, 785–789. [[CrossRef](#)] [[PubMed](#)]
43. Hay, P.J.; Wadt, W.R. Ab Initio Effective Core Potentials for Molecular Calculations. Potentials for K to Au Including the Outermost Core Orbitals. *J. Chem. Phys.* **1985**, *82*, 299–310. [[CrossRef](#)]
44. Hehre, W.J.; Ditchfield, K.; Pople, J.A. Self-Consistent Molecular Orbital Methods. XII. Further Extensions of Gaussian-Type Basis Sets for Use in Molecular Orbital Studies of Organic Molecules. *J. Chem. Phys.* **1972**, *56*, 2257–2261. [[CrossRef](#)]
45. Francl, M.M.; Pietro, W.J.; Hehre, W.J.; Binkley, J.S.; Gordon, M.S.; DeFrees, D.J.; Pople, J.A. Self-Consistent Molecular Orbital Methods. XXIII. A Polarization-Type Basis Set for Second-Row Elements. *J. Chem. Phys.* **1982**, *77*, 3654–3665. [[CrossRef](#)]
46. Tomasi, J.; Mennucci, B.; Cammi, R. Quantum Mechanical Continuum Solvation Models. *Chem. Rev.* **2005**, *105*, 2999–3093. [[CrossRef](#)]
47. Bark, T.; Thummel, R.P. [1,10]-Phenanthroline-2-Yl Ketones and Their Coordination Chemistry. *Inorg. Chem.* **2005**, *44*, 8733–8739. [[CrossRef](#)]

48. Shang, X.; Han, D.; Liu, M.; Zhang, G. A Theoretical Study on the Electronic and Photophysical Properties of Two Series of Iridium(III) Complexes with Different Substituted N₂N Ligand. *RSC Adv.* **2017**, *7*, 5055–5062. [[CrossRef](#)]
49. Han, D.; Zhao, L.; Pang, C.; Zhao, H. The Effect of Substituted Pyridine Ring in the Ancillary Group on the Electronic Structures and Phosphorescent Properties for Ir(III) Complexes from a Theoretical Viewpoint. *Polyhedron* **2017**, *126*, 134–141. [[CrossRef](#)]
50. Shang, X.; Han, D.; Li, D.; Wu, Z. Theoretical Study of Injection, Transport, Absorption and Phosphorescence Properties of a Series of Heteroleptic Iridium(III) Complexes in OLEDs. *Chem. Phys. Lett.* **2013**, *565*, 12–17. [[CrossRef](#)]
51. Shang, X.; Li, Y.; Zhan, Q.; Zhang, G. Theoretical Investigation of Photophysical Properties for a Series of Iridium(III) Complexes with Different Substituted 2,5-Diphenyl-1,3,4-Oxadiazole. *New J. Chem.* **2016**, *40*, 1111–1117. [[CrossRef](#)]
52. Frisch, M.J.; Trucks, G.W.; Schlegel, H.B.; Scuseria, G.E.; Robb, M.A.; Cheeseman, J.R.; Scalmani, G.; Barone, V.; Petersson, G.A.; Nakatsuji, H.; et al. *Gaussian 16*; Gaussian Inc.: Wallingford, CT, USA, 2016.
53. Lu, T.; Chen, F. Multiwfn: A Multifunctional Wavefunction Analyzer. *J. Comput. Chem.* **2012**, *33*, 580–592. [[CrossRef](#)] [[PubMed](#)]
54. Dreyse, P.; González, I.; Cortés-Arriagada, D.; Ramírez, O.; Salas, I.; González, A.; Toro-Labbe, A.; Loeb, B. New Cyclometalated Ir(III) Complexes with Bulky Ligands with Potential Applications in LEC Devices: Experimental and Theoretical Studies of Their Photophysical Properties. *New J. Chem.* **2016**, *40*, 6253–6263. [[CrossRef](#)]
55. Liu, B.; Lystrom, L.; Kilina, S.; Sun, W. Effects of Varying the Benzannulation Site and π Conjugation of the Cyclometalating Ligand on the Photophysics and Reverse Saturable Absorption of Monocationic Iridium(III) Complexes. *Inorg. Chem.* **2019**, *58*, 476–488. [[CrossRef](#)]
56. Coe, B.J.; Helliwell, M.; Raftery, J.; Sánchez, S.; Peers, M.K.; Scrutton, N.S. Cyclometalated Ir(III) Complexes of Deprotonated N-Methylbipyridinium Ligands: Effects of Quaternised N Centre Position on Luminescence. *Dalt. Trans.* **2015**, *44*, 20392–20405. [[CrossRef](#)]
57. Huang, S.F.; Sun, H.Z.; Shan, G.G.; Li, F.S.; Zeng, Q.Y.; Zhao, K.Y.; Su, Z.M. Rational Design and Synthesis of Cationic Ir(III) Complexes with Triazolone Cyclometalated and Ancillary Ligands for Multi-Color Tuning. *Dye. Pigment.* **2017**, *139*, 524–532. [[CrossRef](#)]
58. González, I.; Cortés-Arriagada, D.; Dreyse, P.; Sanhueza-Vega, L.; Ledoux-Rak, I.; Andrade, D.; Brito, I.; Toro-Labbe, A.; Soto-Arriaza, M.; Carmori, S.; et al. A Family of Ir(III) Complexes with High Nonlinear Optical Response and Their Potential Use in Light-Emitting Devices. *Eur. J. Inorg. Chem.* **2015**, *29*, 4946–4955. [[CrossRef](#)]
59. Zhang, Q.; Wang, L.; Wang, X.; Li, Y.; Zhang, J. Tuning the Color and Phosphorescent Properties of Iridium(III) Complexes with Phosphine-Silanolate Ancillary Ligand: A Theoretical Investigation. *Org. Electron.* **2016**, *28*, 100–110. [[CrossRef](#)]
60. Henwood, A.F.; Antón-García, D.; Morin, M.; Rota Martir, D.; Cordes, D.B.; Casey, C.; Slawin, A.M.Z.; Lebl, T.; Bühl, M.; Zysman-Colman, E. Conjugated, Rigidified Bibenzimidazole Ancillary Ligands for Enhanced Photoluminescence Quantum Yields of Orange/Red-Emitting Iridium(III) Complexes. *Dalt. Trans.* **2019**, *48*, 9639–9653. [[CrossRef](#)]
61. Demir, N.; Karaman, M.; Yakali, G.; Gultekin, B.; Tugsuz, T.; Denizalti, S.; Demic, S.; Aygun, M.; Dindar, B.; Can, M. Supramolecular Orange-Red- And Yellow-Emitting Ir(III) Complexes with TFSI and PF6 Counteranions and Production of LEC Devices. *ACS Appl. Electron. Mater.* **2020**, *2*, 3549–3561. [[CrossRef](#)]
62. Yang, X.; Xu, X.; Zhou, G. Recent Advances of the Emitters for High Performance Deep-Blue Organic Light-Emitting Diodes. *J. Mater. Chem. C* **2015**, *3*, 913–944. [[CrossRef](#)]
63. González, I.; Gómez, J.; Santander-Nelli, M.; Natali, M.; Cortés-Arriagada, D.; Dreyse, P. Synthesis and Photophysical Characterization of Novel Ir(III) Complexes with a Dipyrrophenazine Analogue (Pp_{dh}) as Ancillary Ligand. *Polyhedron* **2020**, *186*, 114621. [[CrossRef](#)]
64. Chang, C.H.; Wu, Z.J.; Chiu, C.H.; Liang, Y.H.; Tsai, Y.S.; Liao, J.L.; Chi, Y.; Hsieh, H.Y.; Kuo, T.Y.; Lee, G.H.; et al. A New Class of Sky-Blue-Emitting Ir(III) Phosphors Assembled Using Fluorine-Free Pyridyl Pyrimidine Cyclometalates: Application toward High-Performance Sky-Blue- and White-Emitting OLEDs. *ACS Appl. Mater. Interfaces* **2013**, *5*, 7341–7351. [[CrossRef](#)] [[PubMed](#)]
65. Chen, Y.; Liu, C.; Wang, L. Effects of Fluorine Substituent on Properties of Cyclometalated Iridium(III) Complexes with a 2,2'-Bipyridine Ancillary Ligand. *Tetrahedron* **2019**, *75*, 130686. [[CrossRef](#)]
66. González, I.; Natali, M.; Cabrera, A.R.; Loeb, B.; Maze, J.; Dreyse, P. Substituent Influence in Phenanthroline-Derived Ancillary Ligands on the Excited State Nature of Novel Cationic Ir(III) Complexes. *New J. Chem.* **2018**, *42*, 6644–6654. [[CrossRef](#)]
67. Yu, G.X.; Lin, C.H.; Liu, Y.X.; Yi, R.H.; Chen, G.Y.; Lu, C.W.; Su, H.C. Efficient and Saturated Red Light-Emitting Electrochemical Cells Based on Cationic Iridium(III) Complexes with EQE up to 9.4%. *Chem.-A Eur. J.* **2019**, *25*, 13748–13758. [[CrossRef](#)]
68. You, Y.; Park, S.Y. Phosphorescent Iridium(III) Complexes: Toward High Phosphorescence Quantum Efficiency through Ligand Control. *Dalt. Trans.* **2009**, 9226, 1267–1282. [[CrossRef](#)]
69. McGown, L.B.; Nithipahkom, K. Molecular Fluorescence and Phosphorescence. *Appl. Spectrosc. Rev.* **2000**, *35*, 353–393. [[CrossRef](#)]
70. Haneder, S.; Da Como, E.; Feldmann, J.; Lupton, J.M.; Lennartz, C.; Erk, P.; Fuchs, E.; Molt, O.; Münster, I.; Schildknecht, C.; et al. Controlling the Radiative Rate of Deep-Blue Electrophosphorescent Organometallic Complexes by Singlet-Triplet Gap Engineering. *Adv. Mater.* **2008**, *20*, 3325–3330. [[CrossRef](#)]
71. Shang, X.; Han, D.; Zhou, D.; Zhang, G. Shedding Light on the Photophysical Properties of Iridium(III) Complexes with a Dicyclopentadienyl Phosphate Ligand via N-Substitution from a Theoretical Viewpoint. *New J. Chem.* **2017**, *41*, 1645–1652. [[CrossRef](#)]
72. Chai, J.D.; Head-Gordon, M. Long-Range Corrected Hybrid Density Functionals with Damped Atom-Atom Dispersion Corrections. *Phys. Chem. Chem. Phys.* **2008**, *10*, 6615–6620. [[CrossRef](#)] [[PubMed](#)]

73. Costa, R.D.; Ortí, E.; Bolink, H.J.; Graber, S.; Housecroft, C.E.; Constable, E.C. Light-Emitting Electrochemical Cells Based on a Supramolecularly-Caged Phenanthroline-Based Iridium Complex. *Chem. Commun.* **2011**, *47*, 3207–3209. [[CrossRef](#)] [[PubMed](#)]
74. Monti, F.; Baschieri, A.; Gualandi, I.; Serrano-Pérez, J.J.; Junquera-Hernández, J.M.; Tonelli, D.; Mazzanti, A.; Muzzioli, S.; Stagni, S.; Roldan-Carmona, C.; et al. Iridium(III) Complexes with Phenyl-Tetrazoles as Cyclometalating Ligands. *Inorg. Chem.* **2014**, *53*, 7709–7721. [[CrossRef](#)] [[PubMed](#)]
75. Yao, R.; Liu, D.; Mei, Y.; Dong, R. Synthesis and Properties of Novel Blue Light-Emitting Iridium Complexes Containing 2',6'-Difluoro-2,3'-Bipyridine Ligands. *J. Photochem. Photobiol. A Chem.* **2018**, *355*, 136–140. [[CrossRef](#)]
76. Reddy, M.L.P.; Bejoymohandas, K.S. Evolution of 2, 3'-Bipyridine Class of Cyclometalating Ligands as Efficient Phosphorescent Iridium(III) Emitters for Applications in Organic Light Emitting Diodes. *J. Photochem. Photobiol. C Photochem. Rev.* **2016**, *29*, 29–47. [[CrossRef](#)]
77. Lee, S.J.; Park, K.M.; Yang, K.; Kang, Y. Blue Phosphorescent Ir(III) Complex with High Color Purity: Fac-Tris(2',6'-Difluoro-2,3'-Bipyridinato-N,C 4')Iridium(III). *Inorg. Chem.* **2009**, *48*, 1030–1037. [[CrossRef](#)]
78. Yang, C.H.; Mauro, M.; Polo, F.; Watanabe, S.; Muenster, I.; Fröhlich, R.; De Cola, L. Deep-Blue-Emitting Heteroleptic Iridium(III) Complexes Suited for Highly Efficient Phosphorescent OLEDs. *Chem. Mater.* **2012**, *24*, 3684–3695. [[CrossRef](#)]
79. Costa, R.D.; Ortí, E.; Bolink, H.J.; Graber, S.; Housecroft, C.E.; Neuburger, M.; Schaffner, S.; Constable, E.C. Two Are Not Always Better than One: Ligand Optimisation for Long-Living Light-Emitting Electrochemical Cells. *Chem. Commun.* **2009**, 2029–2031. [[CrossRef](#)]
80. Cortés-Arriagada, D.; Dreyse, P.; Salas, F.; González, I. Insights into the Luminescent Properties of Anionic Cyclometalated Iridium(III) Complexes with Ligands Derived from Natural Products. *Int. J. Quantum Chem.* **2018**, *118*, e25664. [[CrossRef](#)]
81. Shang, X.; Han, D.; Zhan, Q.; Zhang, G.; Li, D. DFT and TD-DFT Study on the Electronic Structures and Phosphorescent Properties of a Series of Heteroleptic Iridium(III) Complexes. *Organometallics* **2014**, *33*, 3300–3308. [[CrossRef](#)]
82. Hutchison, G.R.; Ratner, M.A.; Marks, T.J. Hopping Transport in Conductive Heterocyclic Oligomers: Reorganization Energies and Substituent Effects. *J. Am. Chem. Soc.* **2005**, *127*, 2339–2350. [[CrossRef](#)] [[PubMed](#)]
83. Li, X.N.; Wu, Z.J.; Si, Z.J.; Zhang, H.J.; Zhou, L.; Liu, X.J. Injection, Transport, Absorption and Phosphorescence Properties of a Series of Blue-Emitting Ir(III) Emitters in OLEDs: A DFT and Time-Dependent Dft Study. *Inorg. Chem.* **2009**, *48*, 7740–7749. [[CrossRef](#)] [[PubMed](#)]